Simultaneous Heat and Mass Transfer in Free Convection with Opposing Body Forces

J. A. ADAMS and P. W. McFADDEN

Purdue University, Lafayette, Indiana

An experimental technique which utilized a Mach-Zehnder interferometer was used to measure local heat and mass transfer coefficients during simultaneous heat and mass transfer. The experimental model was a vertical, subliming surface of p-dichlorobenzene. The body force created by the heavy organic vapor in the boundary layer opposed the upward thermal body force caused by heating the surface.

The results indicated that the heat and mass transfer, under the influence of opposing body forces over the range investigated, was from 10 to 15% lower than the values predicted by present approximate analytical solutions for a constant wall heat flux boundary condition.

Simultaneous heat and mass transfer in free convection has been investigated analytically by Somers (*1*), Wilcox (*2*), Eichhorn (*3*), Nakamura (*4*), Mathers et al. (*5*), and others. Experimental investigations include work done by Mathers et al. (*5*) and Bedingfield and Drew (*6*). The analytical work done by Somers (*1*) and Wilcox (*2*) consisted of the integral technique as applied to a binary boundary layer. The approximate solutions obtained required assumptions concerning the boundary-layer profiles of velocity, temperature, and concentration. Eichhorn's solution (*3*) did not involve the conservation of species equation. Nakamura's work included the assumption that the body force was only a function of the temperature difference. The solution of Mathers et al. was obtained by neglecting the nonlinear convection terms. Most experimental investigations of combined heat and mass transfer have been concerned with measurements of average coefficients of heat and mass transfer. A few local values have been obtained by measuring the local changes of geometry in the surface undergoing simultaneous heat and mass transfer.

The purpose of the present investigation was to make local measurements of the coefficients during a process of simultaneous heat and mass transfer. The system and experiments were designed such that the body force due to the temperature difference was approximately the same as the body force caused by the mass transfer from a subliming surface. Of particular interest was the behavior of the free convection boundary layer under the influence of opposing body forces. The term *body force* as used here refers to the buoyant forces on a fluid element within the boundary layer. The body forces are called *opposing* because the downward body force, caused by the subliming organic, acts in a direction opposite to that of the thermal body force caused by the temperature difference between the surface and surroundings. A sketch of the physical model appears in Figure 1. With the experimental procedure employed, it was not necessary to measure local changes in the geometry of the subliming surface in order to obtain local mass transfer coefficients. The subliming surface was placed in the light path of a Mach-Zehnder

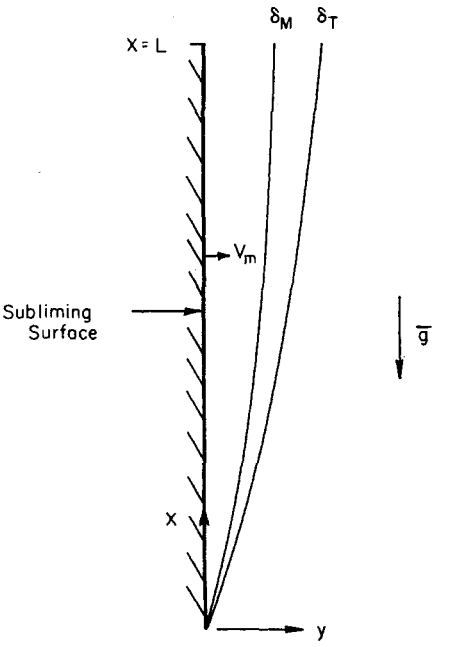

Fig. 1. Physical model.

J. A. Adams is at the U. S. Naval Academy, Annapolis, Maryland.

interferometer, which has been used several times to study heat transfer. Eckert has reported many such investigations, for example, reference 7. The advantage of the interferometer is that local changes in density can be measured accurately by relating the change of index of refraction to the change in density by means of the Gladstone-Dale equation. The simultaneous heat and mass transfer caused changes in the index of refraction within the boundary layer. These changes in index of refraction, which resulted in initially horizontal fringes being shifted within the boundary layer, were recorded on Polaroid film. These fringe shifts were related to the thermodynamic properties of temperature and organic partial pressure. By measuring simultaneously the local fringe shifts with the interferometer, and the local temperature with a thermocouple probe, the local boundary-layer profiles of temperature and organic partial pressure were determined. The local values of the heat and mass transfer coefficients were then determined from the measured profiles.

APPARATUS AND PROCEDURE

The design and selection of the experimental apparatus were largely dependent on the fact that optical methods of measurement were to be used. The size and structure of the test section had to be compatible with the interferometer, in addition to providing the phenomenon of combined heat and mass transfer which was to be investigated.

The test section consisted of a vertical, electrically heated, stainless steel plate which was coated with a thin layer of *p*-dichlorobenzene. The plate was 22.8 cm. high and 61.0 cm. long. The thickness of the stainless steel plate was 3.18 mm. The electrical energy necessary for heating the plate was supplied by a high-current, low-voltage transformer. Buss bars, which were 1.8 cm. sq. and 28 cm. long, were attached to each end of the plate on the back side. The electrical cables from the transformer were attached to the buss bars. In order to reduce end loss, separate heaters were installed in each of the buss bars. The organic coating was 2.5 mm. thick and was formed by pouring the liquid organic onto the plate and letting it solidify. Before coating, the plate was carefully leveled in a horizontal position and a frame was attached around the edges to hold the liquid organic in place until a solid smooth surface was formed.

The Mach-Zehnder interferometer consisted of mirrors and beam splitters which had a diameter of 25.4 cm. A mercury arc light was used, along with the required filters, to produce a wavelength of 5,461 Å. Spatial coherence was obtained by focusing the light onto a pinhole which served as the light source for the interferometer. The image of the test section was focused on a camera which included a holder for Polaroid film.

The interferometer was adjusted so that horizontal fringes were formed before the coated plate was placed in the light path of the interferometer. Then, the coated vertical plate was aligned such that the light passed parallel to the length of the plate. When a coated plate was set in the interferometer light path, but before the plate was heated, the horizontal fringes were shifted as shown in Figure 2*A*. Fringe shifts formed by a heated, uncoated plate are shown in Figure 2*B*. These shifts were due to the change of index of refraction within the boundary layer caused by the subliming organic vapor in Figure 2*A* and the heated air in Figure 2*B*. These fringe shifts were recorded with Polaroid film. When the coated plate was heated to a temperature above the environmental temperature, the index of refraction was changed, due to both the concentration of the organic vapor and the increased temperature in the boundary layer. Typical photographs are illustrated by the sketches in Figures 2*C* and 2*D*. The organic vapor increased the index of refraction, whereas the heated air produced a smaller index of refraction. Thus, the fringe shifts caused by the organic vapor were in the opposite direction from those caused by the heated air.

The tests of simultaneous heat and mass transfer were performed by heating the coated plate. When the wall temperature was 5°C. above the environmental temperature, the initially horizontal fringes were only slightly displaced as shown

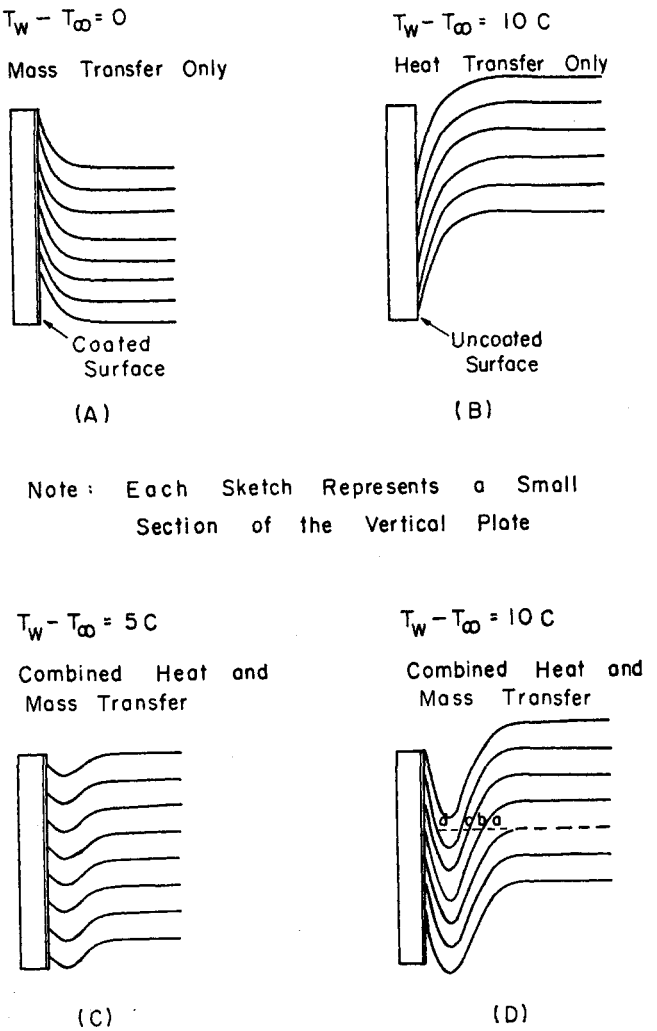

Fig. 2. Interferograms.

in Figure 2*C*. As the temperature of the wall was increased, the fringe shifts also changed, due to both the increased sublimation rate and the increased temperature within the boundary layer. A typical photograph for a wall temperature of 10°C. above the environmental temperature is illustrated in Figure 2*D*.

An optical comparator was used to measure the fringe shifts from the photographs. This instrument made it possible to measure to an accuracy of ± 0.10 fringe shifts. The method of counting the fringe shifts is shown by the dashed line in Figure 2*D*. The counting was done from right to left, relative to the undisturbed horizontal fringes outside the boundary layer. The first intersection *a* records a fringe shift of —1.0. The second intersection *b* records a fringe shift of —2.0. The third intersection *c* records a fringe shift of —3.0. Notice that intersection *d* lies on the same fringe as intersection *c*, and the fringe shift at this location is also —3.0. The next intersection records a fringe shift of —2.0, and the total fringe shift at the wall is seen to be —1.0 at this specific vertical location on the plate.

The relationship between the fringe shift and change in index of refraction is given by

$$S = \frac{l}{\lambda}\{[n(x,y) - 1] - [n_i - 1]\} \qquad (1)$$

Since only air was initially present, n_i was the index of refraction of the air outside the boundary layer during the heat and mass transfer process. For gases the molar refractivity $\bar{R}$ is given by the following expression:

$$\bar{R} = \frac{2}{3}(n - 1)\frac{M}{\rho}, \qquad (2)$$

and the Gladstone-Dale constant K is defined as

$$K = \frac{n-1}{\rho} \tag{3}$$

For a mixture of two perfect gases, that is, air and p-dichlorobenzene, the total molar refraction was expressed as

$$\overline{R} = \frac{C_a}{C}\overline{R}_a + \frac{C_b}{C}\overline{R}_b \tag{4}$$

By combining Equations (3) and (4) and using the fact that $\rho = MC$, the following relationship was obtained.

$$(n-1) = (n_a-1) + (n_b-1) \tag{5}$$

By combining Equations (1) and (5), the expression for fringe shift becomes

$$S = \frac{l}{\lambda}\left[(n_a-1) + (n_b-1) - (n_{a,i}-1) - (n_{b,i}-1)\right] \tag{6}$$

By using the Gladstone-Dale relationships for air and p-dichlorobenzene

$$K_a = \frac{n_a-1}{\rho_a}; \quad K_b = \frac{n_b-1}{\rho_b} \tag{7}$$

Equation (6) became

$$S = \frac{l}{\lambda}\left[(K_a\rho_a + K_b\rho_b) - (K_a\rho_{a,i} + K_b\rho_{b,i})\right] \tag{8}$$

For the cases studied in the present work the initial density of component b was zero. This fact, together with the perfect gas relationship, was used to obtain the following expression.

$$S = \frac{l}{\lambda}\left[\frac{K_aP_a}{R_aT} + \frac{K_bP_b}{R_bT} - K_a\rho_{a,i}\right] \tag{9}$$

The total pressure throughout the boundary layer was assumed constant. Thus

$$P = P_a + P_b = \text{constant} \tag{10}$$

By solving for P_a in Equation (10), substituting this expression for P_a into (9), and rearranging the results, the expression for the local partial pressure of the organic vapor was obtained, namely

$$P_b = \frac{\dfrac{TS\lambda}{l} + TK_a\rho_{a,i} - \dfrac{K_aP}{R_a}}{\left(\dfrac{K_b}{R_b} - \dfrac{K_a}{R_a}\right)} \tag{11}$$

As can be seen by Equation (11), the local temperature must be known, in addition to the local fringe shift, in order to calculate local values of partial pressure.

A thermocouple probe for measuring the boundary-layer temperature profiles was constructed in a manner similar to that described by Schechter and Isbin (8) as well as by Schmidt and Beckmann (9). The copper-constantan wire used to make the probes had a diameter of 0.076 mm. and was supported by two hypodermic needles which were 10 cm. apart. The thermocouple junction was formed by soldering the wires together end to end, and was located midway between the tips of the two needles. The thermocouple wires approached the junction along essentially an isotherm. A micrometer head was used to translate the probe perpendicular to the plate within the boundary layer. The probe was calibrated to the nearest 0.1° C. by means of a thermostatically controlled, constant-temperature water bath. It was found that the surface temperature could accurately be determined by linearly extrapolating the temperature measurements made with the boundary-layer probe at distances less than 2 mm. from the surface. This was verified by using embedded thermocouples in the surface of the coated plate. It was also verified during preliminary tests on an uncoated plate when the surface temperatures were measured with embedded thermocouples, with the boundary-layer probe, and by counting the fringe shifts on an interferogram and then calculating the surface temperatures.

During a test at a constant wall heat flux, the coated plate was heated at predetermined values of plate current and buss bar heater currents. After steady state was reached, the boundary-layer temperature profile was measured at twelve different locations and twelve photographs of the fringe shifts were taken. Three thermal boundary-layer traverses were made at each of four vertical locations. The vertical locations were $X/L = 0.77$, $X/L = 0.60$, $X/L = 0.43$, and $X/L = 0.26$, where X was measured from the lower edge of the plate and the height of the plate L was 22.8 cm. At each of the vertical locations, the temperature profile was measured at a location midway between the ends of the plate and at locations 15.2 cm. on each side of this center position. The distance between temperature readings in the boundary layer was 0.635 mm. and the number of separate temperature measurements made in each boundary-layer traverse was between fifteen and eighteen. The average of the three temperature profiles for each of the four vertical locations was obtained, along with the average fringe shift profiles. From these average values, the organic partial pressure profiles were calculated with Equation (11). Representative temperature and partial pressure profiles obtained during one run are shown in Figures 3 and 4.

Certain errors were inherent in the experimental procedure. The interferometric errors which were evaluated were end effects, effects due to the isothermal buss bars, and refraction errors. The thermocouple probe was subjected to radiation and conduction errors. The total error in the fringe shift data ranged between 2 and 4%. The error in the measurement of the temperature difference was less than 1%. Corrections to the data were made to account for these sources of error. For a complete discussion of the experimental errors involved, see reference *10*.

In addition to the fringe shift and temperature measurements in the boundary layer, the total pressure and initial air temperature were measured and the initial air density was calculated. The other terms in Equation (11) were known constants. A complete discussion on how these constants were determined for air and p-dichlorobenzene can be found in reference *10*. Local partial pressure profiles were calculated with Equation (11) for wall temperatures up to the melting point of p-dichlorobenzene (53°C.).

The local Nusselt and Sherwood numbers were found directly from the profiles of temperature and partial pressure, which were plotted with the distance from the wall as the abscissa. One can write

$$q_w = k\left(\frac{dT}{dy}\right)_w \equiv h\Delta T \tag{12}$$

and

$$N_{Nu,x} = \frac{hX}{k} = \frac{X}{\Delta T}\left(\frac{dT}{dy}\right)_w = \frac{X}{\dfrac{\Delta T}{\left(\dfrac{dT}{dy}\right)_w}} = \frac{X}{Y_t} \tag{13}$$

where X is the vertical location on the plate and Y_t is the intersection of the abscissa with the slope at the wall. In a similar manner, $N_{Sh,x} = \dfrac{X}{Y_m}$ (see Figure 4).

RESULTS

The results of the measured local heat and mass transfer coefficients are given in terms of Nusselt and Sherwood numbers. For example, the measured $N_{Nu,x}$ and $N_{Sh,x}$, obtained from the profiles in Figure 3 and 4, are given in Table 1. A comparison between the experimental results and the analytical solutions of Somers (*1*) and

TABLE 1. MEASURED $N_{Nu,x}$ AND $N_{Sh,x}$

X/L	X, mm.	Y_t, mm.	$N_{Nu,x}$	Y_m, mm.	$N_{Sh,x}$
0.77	171	8.20	20.8	4.75	36.0
0.43	95.5	7.80	12.2	4.25	22.4

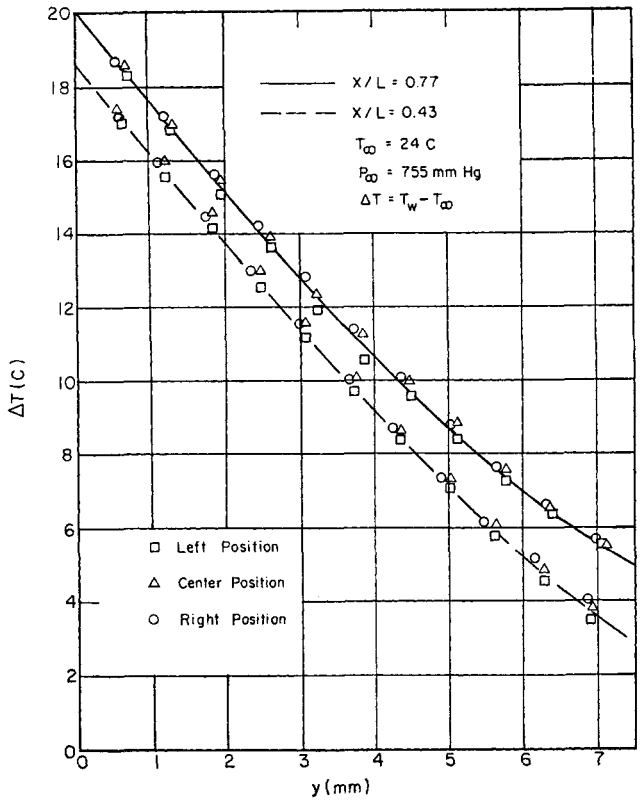

Fig. 3. Average temperature profiles.

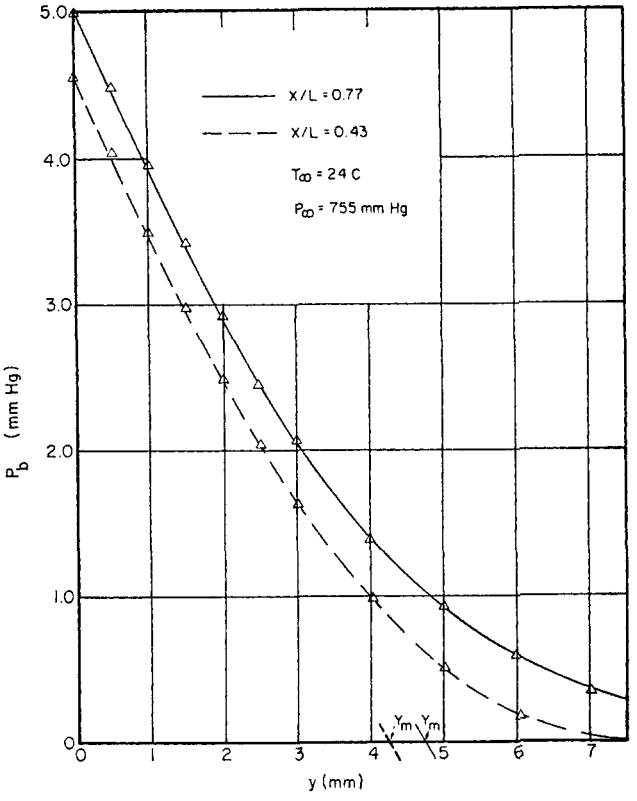

Fig. 4. Average partial pressure profiles.

Wilcox (*2*) is given in Figure 5. The correlations are identified in Table 2. It should be pointed out that the blowing rate of *p*-dichlorobenzene produced at the wall by the subliming surface was small. The maximum normal velocity (v_w) obtained at the wall was 0.38 cm./sec. The Schmidt number of *p*-dichlorobenzene was 2.23.

The analytical results were increased by a factor a 1.14 to take into account the constant heat flux boundary condition. This factor was taken from the results given by Sparrow and Gregg (*11*). Since the constant flux boundary condition was assumed, it was important to verify that this was the actual case. Initial tests on an uncoated plate indicated that the plate closely approached the boundary condition of constant heat flux. Conduction in the plate and nonuniform radiation from the plate made it impossible to obtain exactly a boundary condition of constant wall heat flux, even when uniform heat generation occurred in the wall. Results showed that this boundary condition was even more closely approximated with a plate coated with *p*-dichlorobenzene. Figure 6 gives a comparison between the measured profiles of temperature and partial pressure and the theoretical profiles for the boundary conditions of constant heat flux and constant mass flux. The theoretical profiles were taken from reference *11*. As can be seen, very close agreement was obtained between the measured and the theoretical profiles. These results support the opinion that the measured values of $N_{Nu,x}$ and $N_{Sh,x}$, which were 10 to 15% lower than the predicted values of Somers and Wilcox, were low because of the boundary-layer characteristics, not because of an improper assumption as to the existing boundary conditions at the plate surface. It was also shown (*10*) that the variation of the wall temperature with X closely approximated the case of constant wall heat flux.

The subliming organic surface had the effect of increasing the density of the fluid in the boundary layer, since the molecular weight of *p-dichlorobenzene* was about five times that of air. This opposing body force reduced the sensible heat transfer as compared with the case of a nonsubliming wall. The ratio of the downward body force to the total body force is shown in Figure 7 as a function of $(T_w - T_\infty)$. Note that a minimum was reached near $(T_w - T_\infty)$ equal to 15°C. Also shown in Figure 7 is the variation of $N_{Gr,x}^*$ as a function of $(T_w - T_\infty)$, where

Table 2. Theoretical Correlations

Wilcox: Finite-wall velocity and parabolic profiles (u, T, C)

$$\text{Curve 4: } N_{Nu,x} = 0.435\left[N_{Gr,x} + \sqrt{\frac{N_{Pr}}{N_{Sc}}}\,N_{Gr,x}'\right]^{1/4}$$

$$\text{Curve 1: } N_{Sh,x} = \sqrt{\frac{N_{Sc}}{N_{Pr}}}\,N_{Nu,x}$$

Somers: Finite-wall velocity (v) and polynomial profiles (u, T, C)

$$\text{Curve 5: } N_{Nu,x} = 0.422\left[N_{Gr,x} + \sqrt{\frac{N_{Pr}}{N_{Sc}}}\,N_{Gr,x}'\right]^{1/4}$$

$$\text{Curve 2: } N_{Sh,x} = \sqrt{\frac{N_{Sc}}{N_{Pr}}}\,N_{Nu,x}$$

Wilcox: Zero-wall velocity (v) and polynominal profiles (u, T, C)

$$\text{Curve 6: } N_{Nu,x} = 0.388\left[N_{Gr,x} + \sqrt{\frac{N_{Pr}}{N_{Sc}}}\,N_{Gr,x}'\right]^{1/4}$$

$$\text{Curve 3: } N_{Sh,x} = \sqrt{\frac{N_{Sc}}{N_{Pr}}}\,N_{Nu,x}$$

$$N_{Gr,x}^{*} = \frac{gx^3}{\nu^2}\left[\frac{T_w - T_\infty}{T_\infty} - \frac{T_w}{T_\infty}\left(\frac{M_b - M_a}{M_a}\right)\left(\frac{P_{b,w}}{P}\right)\right] \quad (14)$$

This form of the Grashof number was derived by Merk (*12*). Note that $N_{Gr,x}^{*}$ began to decrease at a value of $(T_w - T_\infty) = 21°C$. After the maximum value of the Grashof number was reached, the Grashof number, and thus the Nusselt and Sherwood numbers, decreased, even though the wall temperature increased. Thus, the local heat transfer coefficient and the local mass transfer coefficient were decreased in value as the temperature difference $(T_w - T_\infty)$ was increased above 21°C. However, as the Grashof number continues to decrease in value, a region will be reached where boundary-layer type of flow will not exist. Whether this value will occur at a Grashof number around 10^4 was not experimentally verified.

Experimental data were replotted in Figure 8 and compared to the following correlations:

$$N_{Sh,x} = 0.475\left[N_{Gr,x}^{*} \cdot \frac{N_{Sc}}{N_{Pr}}\right]^{1/4}$$

$$N_{Nu,x} = 0.475\left[N_{Gr,x}^{*} \cdot \frac{N_{Pr}}{N_{Sc}}\right]^{1/4} \quad (15)$$

These correlations could also be expressed in terms of the Lewis number, defined as $N_{Le} = (N_{Sc})/(N_{Pr})$. The constant (0.475) was obtained as follows. For local values of $N_{Nu,x}$, considering heat transfer from an isothermal wall, the constant is (0.555) (3/4) = 0.416. It was assumed that the ratio of Nusselt number for constant wall heat flux to Nusselt number for constant wall temperature was the same for the case of simultaneous heat and mass transfer as it was for the case of heat transfer. Thus, from the results of Sparrow and Gregg (*11*), the value of the constant was increased by a factor of 1.14 to take into account the constant heat flux boundary condition. Thus, (0.416) (1.14) = 0.475. All experimental points lie with-

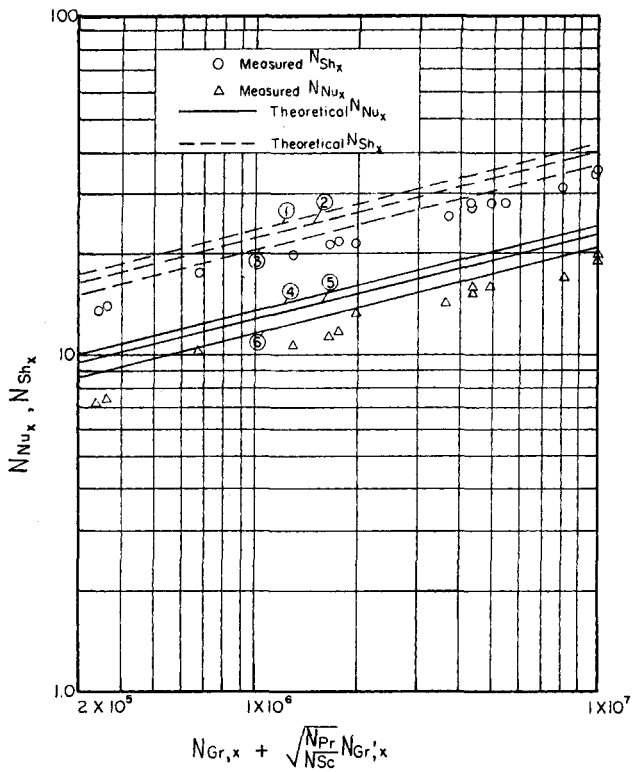

Fig. 5. Theoretical correlations.

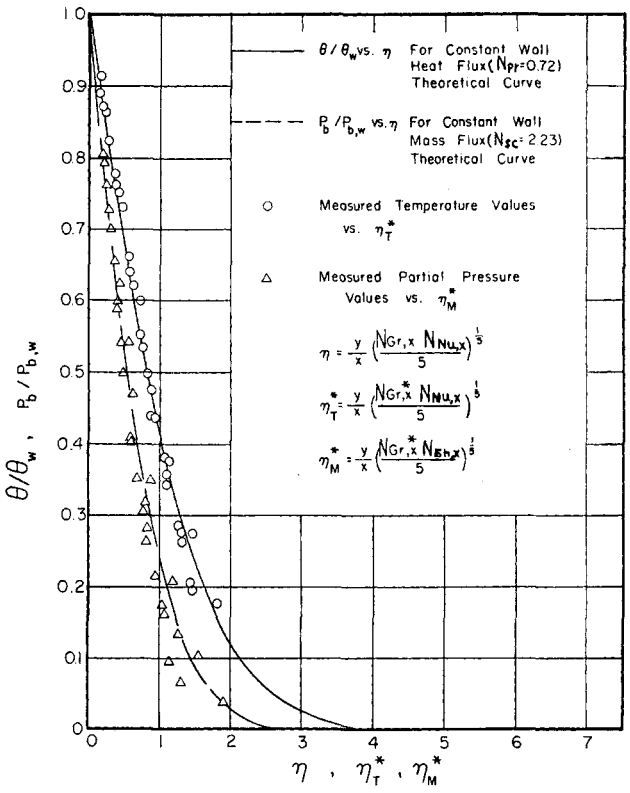

Fig. 6. Dimensionless profiles.

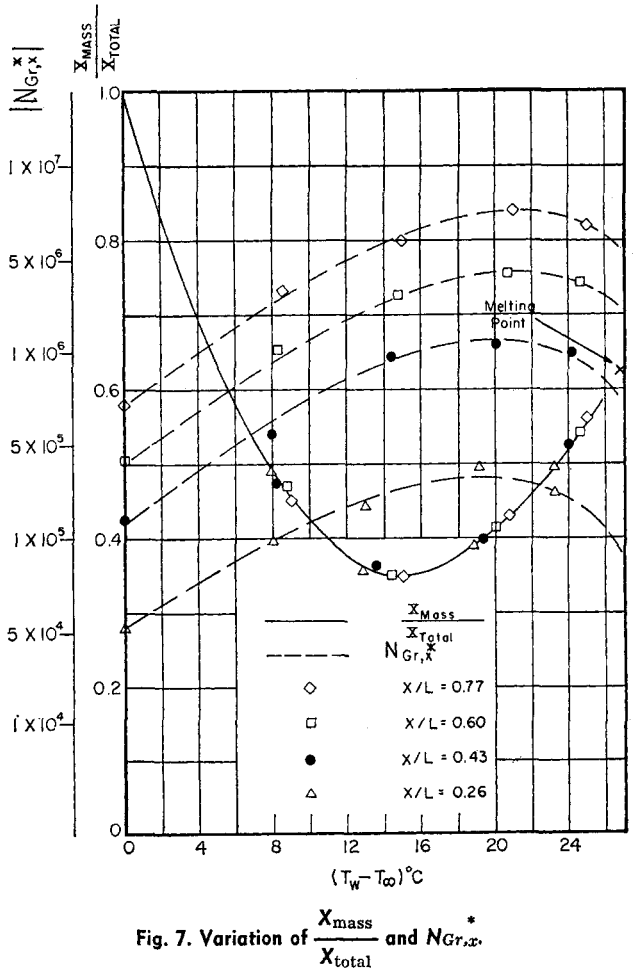

Fig. 7. Variation of $\frac{X_{mass}}{X_{total}}$ and $N_{Gr,x}^{*}$.

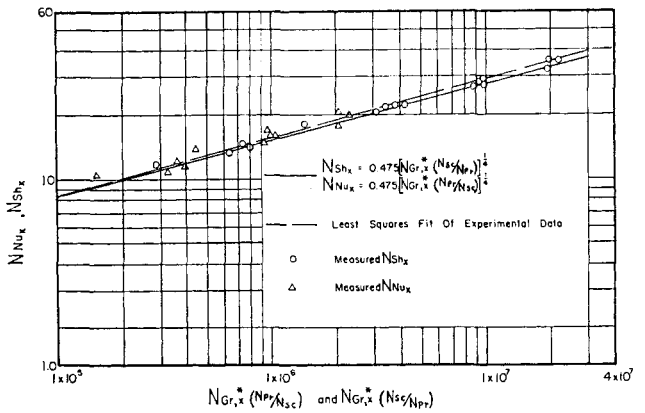

Fig. 8. Experimental correlation.

in ± 10% of the above correlations. A least squares approximation is shown by the dashed line in Figure 8. The equation of the least squares fit was

$$N_{Nu,x} = 0.425\left[N_{Gr,x}^{*}\left(\frac{N_{Pr}}{N_{Sc}}\right)\right]^{0.262} \qquad (16)$$

The average values of the Sherwood and Nusselt numbers can be found from Equation (15) by evaluating $N_{Gr,x}^{*}$ at $x = L$, and multiplying the constant (0.475) by (4/3).

In conclusion, the use of the interferometer to study problems of simultaneous heat and mass transfer proved to be an important experimental technique. The results showed a deviation from the approximate analytical predictions which would have been difficult to measure with less accurate instrumentation. The use of the combined Grashof number $N_{Gr,x}^{*}$ to correlate the data provided an important refinement to existing correlations. Also, the use of this Grashof number, along with correlations similar to the above, should provide accurate predictions of the heat and mass transfer rates for other systems, such as simultaneous heat and mass transfer from a horizontal surface.

ACKNOWLEDGMENT

Dr. J. A. Adams is grateful for the financial assistance provided by a twelve-month NSF Traineeship and a summer grant from the Procter and Gamble Company. The efforts of Dr. W. H. Stevenson, who was responsible for the optical design of the interferometer, are acknowledged. The authors also acknowledge the support provided by Purdue University.

NOTATION

C = concentration
D_{ab} = molecular diffusivity of p-dichlorobenzene into air
g = acceleration due to gravity
h = local heat transfer coefficient
h_m = local mass transfer coefficient
k = thermal conductivity
K = Gladstone-Dale constant
l = total length of plate along direction of light path
L = total height of plate
M = molecular weight
n = index of refraction
P = total pressure
q = power generation from electrical dissipation
$\overline{R}$ = molar refractivity
R = gas constant
S = fringe shift
T = temperature
u = X direction velocity
v = Y direction velocity
X = vertical coordinate along plate surface
$\overline{X}$ = body force
Y = horizontal coordinate perpendicular to plate surface

$$Y_t = \frac{\Delta t}{\left(\frac{dT}{dy}\right)_w}$$

$$Y_m = \frac{\Delta P}{\left(\frac{dP}{dy}\right)_w}$$

Greek Letters

α = concentration densification coefficient = $(1/\rho)/(\partial\rho/\partial C)_T$
β = temperature densification coefficient = $(1/\rho)/(\partial\rho/\partial T)_C$
δ_M = mass boundary-layer thickness
δ_T = thermal boundary-layer thickness
η = dimensionless parameter defined in Figure 6
λ = monochromatic wavelength of light
ν = kinematic viscosity
ρ = density

Subscripts

a = air
b = organic compound, p-dichlorobenzene
i = initial value
m = mass boundary layer
t = thermal boundary layer
w = wall value
∞ = environmental conditions

Nondimensional Parameters

$N_{Gr,x}$ = heat transfer Grashof number = $\frac{g x^3 \beta}{\nu^2}(T_w - T_\infty)$

$N_{Gr,x}'$ = mass transfer Grashof number = $\frac{g x^3 \alpha}{\nu^2}(C_w - C_\infty)$

$N_{Gr,x}^{*}$ = combined Grashof number = $\frac{g x^3}{\nu^2}\left[\frac{T_w - T_\infty}{T_\infty} - \frac{T_w}{T_\infty}\left(\frac{M_b - M_a}{M_a}\right)\frac{P_{b,w}}{P}\right]$

N_{Le} = Lewis number = $\alpha/(D_{ab})$
N_{Pr} = Prandtl number = ν/α
N_{Sc} = Schmidt number = $\nu/(D_{ab})$
$N_{Nu,x}$ = local Nusselt number = $(hX)/k$
$N_{Sh,x}$ = local Sherwood number = $(h_m X)/(D_{ab})$

LITERATURE CITED

1. Somers, E. V., *J. Appl. Mech.*, **23**, 295 (1956).
2. Wilcox, W. R., *Chem. Eng. Sci.*, **13**, 3, 113 (1961).
3. Eichhorn, R., *J. Heat Transfer*, **82**, No. 3, 260 (August, 1960).
4. Nakamura, H., *J. Soc. Mech. Engrs.*, **5**, 18 (1962).
5. Mathers, W. G., A. J. Madden, and E. L. Piret, *Ind. Eng. Chem.*, **49**, 961 (1957).
6. Bedingfield, C. H., and T. B. Drew, *ibid.*, **42** (1950).
7. Eckert, E. R. G., and E. E. Soehngen, *AF Tech. Rept. 5747* (December, 1948).
8. Schechter, R. S., and H. S. Isbin, *A.I.Ch.E. J.*, **4**, 81 (1958).
9. Schmidt, E., and W. Beckman, *Tech. Mech. Thermodynamik*, **1**, No. 10 (October, 1930).
10. Adams, J. A., Ph.D. dissertation, Purdue Univ., Lafayette, Ind. (1965).
11. Sparrow, E. M., and J. E. Gregg, *Trans. Am. Soc. Mech. Engrs.*, **78**, 435 (1956).
12. Merk, H. J., *Appl. Sci. Res.*, **4**, 435 (1954).

Manuscript received September 27, 1965; revision received January 19, 1966; paper accepted January 21, 1966.